Using Satellite Altimetry to Calibrate the Simulation of Typhoon Seth Storm Surge off Southeast China

Xiaohui Li [1], Guoqi Han [2,*], Jingsong Yang [1,*] , Dake Chen [1], Gang Zheng [1] and Nan Chen [3,4]

[1] State Key Laboratory of Satellite Ocean Environment Dynamics, Second Institute of Oceanography, State Oceanic Administration, Hangzhou 310012, China; lixiaohui1991@live.cn (X.L.); dchen@sio.org.cn (D.C.); zhenggang@sio.org.cn (G.Z.)

[2] Fisheries and Oceans Canada, Northwest Atlantic Fisheries Centre, St. John's, NL A1C 5X1, Canada

[3] State Key Laboratory of Marine Environmental Science, Xiamen University, Xiamen 361005, China; chennan@udel.edu

[4] Center for Remote Sensing, College of Earth, Ocean and Environment, University of Delaware, Newark, DE 19716, USA

* Correspondence: guoqi.han@dfo-mpo.gc.ca (G.H.); jsyang@sio.org.cn (J.Y.); Tel.: +1-709-772-4326 (G.H.)

Abstract: Satellite altimeters can capture storm surges generated by typhoons and tropical storms, if the satellite flies over at the right time. In this study, we show TOPEX/Poseidon altimeter-observed storm surge features off Southeast China on 10 October 1994 during Typhoon Seth. We then use a three-dimensional, barotropic, finite-volume community ocean model (FVCOM) to simulate storm surges. An innovative aspect is that satellite data are used to calibrate the storm surge model to improve model performance, by adjusting model wind forcing fields (the National Center for Environment Prediction (NCEP) reanalysis product) in reference to the typhoon best-track data. The calibration reduces the along-track root-mean-square (RMS) difference between model and altimetric data from 0.15 to 0.10 m. It also reduces the RMS temporal difference from 0.21 to 0.18 m between the model results and independent tide-gauge data at Xiamen. In particular, the calibrated model produces a peak storm surge of 1.01 m at 6:00 10 October 1994 at Xiamen, agreeing with tide-gauge data; while the peak storm surge with the NCEP forcing is 0.71 m only. We further show that the interaction between storm surges and astronomical tides contributes to the peak storm surge by 34% and that the storm surge propagates southwestward as a coastally-trapped Kelvin wave.

Keywords: storm surge; satellite altimetry; calibration; numerical modelling; FVCOM

1. Introduction

Storm surges, generated by extreme wind stress acting on shallow, continental shelf seas, can lead to severe coastal floods, particularly when they coincide with a high astronomic tide [1]. They can result in devastating economic and social impacts, including loss of life, damage to property and disruption of essential services [2–5]. As climate changes, coastal areas are becoming increasingly more vulnerable to storm surges [4]. To mitigate loss of life and damage to property by storm surges, great efforts have been made in monitoring and forecasting storm surges, such as enhancing tide-gauge networks, integrating satellite observations and improving numerical prediction of storm surge and inundation [6].

In recent years, some studies have indicated that satellite altimetry is capable of observing and studying storm surge features. Scharroo et al. showed that Geosat follow-on sea level anomalies reached 90 cm at the coast of the Gulf of Mexico during Hurricane Katrina [7]. Han et al. clearly showed the utility of satellite altimetry in observing and understanding storm surges, complementing

tide-gauge observations for the analysis of storm surge characteristics and for the validation and improvement of storm surge models [4]. Lillibridge et al. reported that the storm surge caused by Hurricane Sandy was captured by the HaiYang-2A (HY-2A) satellite [8]. Recently, Chen et al. showed a detailed analysis of HY-2A satellite observations combined with tide-gauge data during the passage of Sandy. For this event, Montauk's tide-gauge recorded a maximum surge of 173 cm, and HY-2A showed positive sea-level anomalies of about 183 cm during the storm event. Further analysis suggests that the continental shelf wave generated during the passage of Sandy and observed by altimetry and tide-gauges has a propagating speed of 6.5 m/s [6]. The SARAL/Altika altimeter captured a storm surge event in the North Sea during Cyclone Xaver in December 2013 [9]. Han et al. studied storm surge features in the Gulf of Mexico during Hurricane Isaac, as observed by Jason-1 and Jason-2 altimeters and tide-gauge data, showing the utility of the constellation of altimeter missions and prospects of the upcoming Surface Water and Ocean Topography (SWOT) mission [10]. These studies have shown that satellite altimetry is very useful for observing and understanding features of storm surges. They have also indicated that it is highly opportunistic for a single satellite altimetry mission to capture storm surges due to infrequent sampling. Satellite altimetry does not provide along-coast sea surface height distribution. On the other hand, there are a few recent studies on using satellite altimetry data to improve storm surge simulation through data assimilation [11–13]. These studies [11–13] showed the positive impacts and challenges of assimilating altimetry data on storm surge hindcasts and forecasts in the Gulf of Venice.

Typhoons often cause storm surges off the eastern and southern coasts of China in summer and fall, for example along the coast of Fujian. Taiwan Strait, connecting the South China Sea and the East China Sea (Figure 1), is a shallow water area between Fujian and Taiwan, with an average depth of about 60 m [14]. The tide is very strong and dominated by semi-diurnal constituents [14–16]. Storm surge models have been developed for Taiwan Strait and adjacent waters [16,17]. According to previous studies, the interaction between tide and storm surge is notable, especially in shallow waters where tidal range is large [18–20]. In spite of the fact that the region is often hit by typhoons and storm surges, there has been little literature reporting on storm surges observed by satellite altimetry.
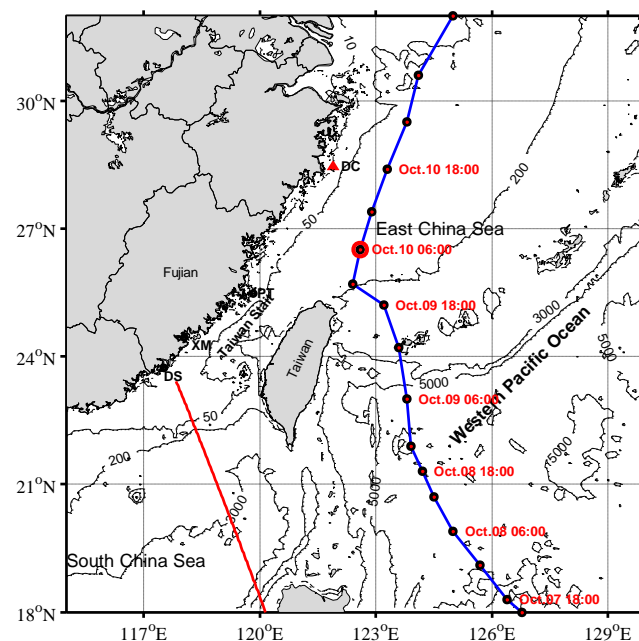

Figure 1. Map showing the study area off Southeast China with bathymetric contours in meters. Typhoon Seth's track and locations at specific times are shown as blue lines and red dots. The red line is the TOPEX/Poseidon (T/P) satellite ground track. Pingtan (PT), Xiamen (XM) and Dongshan (DS) tide stations are marked by circles. The Dachen (DC) weather station is also depicted (red triangle).

In this study, we use TOPEX/Poseidon (T/P) satellite altimetry observations to show cross-shelf variation of Typhoon Seth storm surge off Southeast China on 10 October 1994. The T/P satellite ground track had a pass nearby Xiamen at 05:46 UTC on 10 October 1994 (Figure 1), when Typhoon Seth was located close to the southeastern coast of China. We then apply a state-of-the-art finite-volume community ocean model (FVCOM) [21] to simulate and understand the Typhoon Seth storm surge off Southeast China. The novel aspect of this study is using satellite altimetry observations to calibrate the storm surge model by adjusting the model wind forcing fields. We further integrate the T/P satellite altimetry with the simulated results from the calibrated model to investigate features of the storm surge. Note that storm surges are not only the sea level rises directly forced by wind stress and/or low atmospheric pressure, but also coastally-trapped free propagating signals generated remotely by storms. On 1 October 1994, Seth started in an area near the Marshall Islands and then strengthened into a strong typhoon on 7 October moving northwestward east of Taiwan. As it moved through the Ryukyu Islands, winds gusted to 110 knots (200 km/h). At 00:00 on 10 October, it turned northeastward.

This paper is organized as follows. In Section 2, we describe altimetry data, tide-gauge data, the FVCOM model and its setup, as well as the model calibration procedure. Section 3 evaluates and calibrates the model results against observations. Section 4 discusses tide-surge interactions and the mechanisms of storm surge propagation. We provide conclusions in Section 5.

2. Data and Methods

2.1. T/P Data

The T/P satellite was launched on 10 August 1992. We have used 1-Hz altimetric sea surface height anomalies along a T/P satellite ground track (Track 88) nearby Xiamen, Fujian province (Figure 1). The T/P data were obtained from the Centre for Topographic studies of the Ocean and Hydrosphere (CTOH) X-TRACK product. The altimetric sea surface height anomalies are corrected for ionospheric and tropospheric delays, sea state bias, as well as ocean, solid Earth and pole tides. Inverse barometer or high-frequency dynamic corrections are not applied. The X-TRACK product starts from Geophysical Data Record (GDR) data, with enhancement in geophysical corrections (e.g., the ionospheric correction and the wet tropospheric correction) and thus has more valid data points than a standard GDR product in coastal regions [22]. The X-TRACK sea surface height anomalies are referenced to the mean sea surface calculated from the along-track T/P, Jason-1 and Jason-2 data from 1993 to 2015.

2.2. Tide-Gauge Data

Hourly sea level data at Xiamen (Figure 1) for 1994 are obtained from the University of Hawaii Sea Level Center (UHLSC, http://uhslc.soest.hawaii.edu/). Inverse barometer correction is not applied, since we are interested in storm surge. Harmonic analysis including 59 tidal constituents is carried out to retrieve tidal constants [23]. We subtract the tide height predicted using the retrieved tidal constants from the hourly sea level data to produce non-tidal sea level anomalies.

2.3. FVCOM (3.2.1) Ocean Circulation Model

The model used in this study is FVCOM, which has the advantages of horizontal grid flexibility and computational efficiency [21]. Thus, this model is highly suitable for the present study area with an irregular complex coastline, reaching from shallow waters to the steep topography of the shelf break.

The model domain covers the eastern and southern coast of China and the adjacent deep ocean (Figure 2). With 29,235 unequally-spaced nodes and 56,534 elements, the horizontal grid has a typical resolution of 10 km over the shelf and 2–5 km along the coast and shelf edge. Vertically, 11 levels are uniformly distributed. We use bottom topography from the Earth Topography 1-arc-minute gridded global relief (ETOPO1) dataset [24]. The bathymetry was smoothed to improve the model stability. This technique limits the depth difference for three vertices at each triangle. On the basis of the Courant–Friedrichs–Levy (CFL) numerical stability condition, model equations are solved with an

integration time step of 2 s for the external mode and an internal to external mode ratio of 10. We use the quadratic bottom friction formulation, with a minimum drag coefficient of 0.0025 [21].
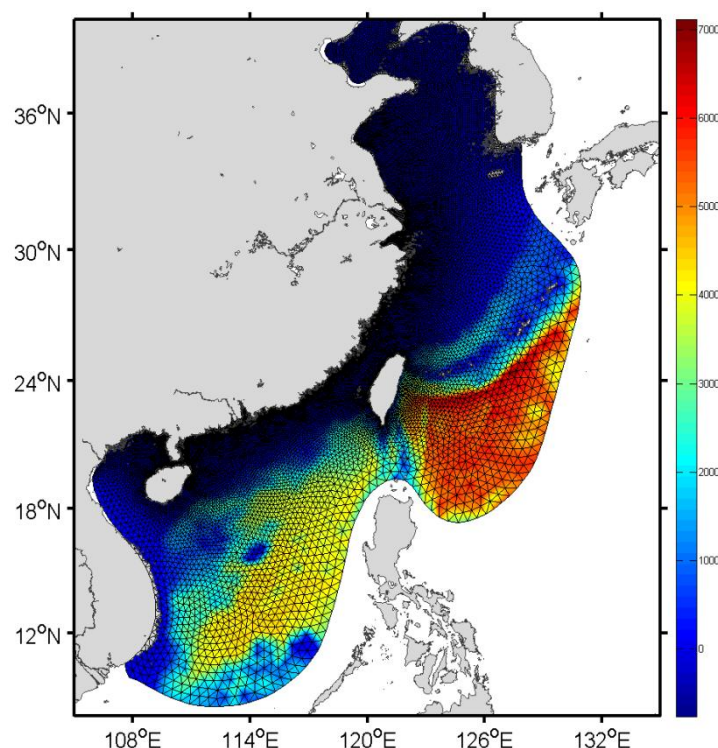

Figure 2. Mesh with 29,235 nodes in the waters off the eastern and southern coast of China. The fine grid resolution is around 2 km along the Taiwan Strait coast.

The model is forced by winds and air pressure at the sea surface. We used 6-hourly, 10-m, 0.25° by 0.25° wind stress and sea level pressure of the National Center for Environmental Prediction (NCEP), from NCAR's RAD (National Center for Atmospheric Research, Research Data Archive, http://rda.ucar.edu/datasets) over the entire computational domain. Tidal heights for the eight main tidal constituents (semi-diurnal (M2, S2, N2 and K2) and diurnal (K1, O1, P1 and Q1)) predicted by OTIS (OSU Tidal Inversion Software) were specified along the open boundaries [25].

The model sea level and velocity were initialized from zero. The model reaches an approximate dynamic equilibrium after running for 15 days. The results from 26 September to 18 October 1994 were analyzed to examine the storm surge.

We carry out the model runs for tide forcing only, for wind forcing only and for tide and wind forcing simultaneously. The non-tidal sea level anomalies were obtained by subtracting the tide level of the model run for tide forcing only from the total sea level of the model run for tide and wind forcing simultaneously.

2.4. Modification of NCEP Winds

A good quality wind field is essential for storm surge calculations [11–13]. However, the wind field from the atmospheric reanalysis product usually underestimates the maximum sustainable wind of hurricanes and typhoons. Various approaches have been used to adjust reanalysis winds in the vicinity of the storm center, for example, by fitting the analytical cyclone model of Holland [26,27] within the radius of maximum wind (*RMW*) and then blending the analytical model wind with the

reanalysis wind field. In this study, we follow their approach, except for not fitting the analytical model. Ignoring the asymmetry of the typhoon, we modify the NCEP wind fields as follows:

$$V_w = (\frac{r}{RMW} \times ntimes + \frac{RMW - r}{RMW}) \times V_{NCEP}, 0 \leq r \leq RMW \tag{1}$$

$$V_w = (\frac{r - RMW}{3 \times RMW} + \frac{4 \times RMW - r}{3 \times RMW} \times ntimes) \times V_{NCEP}, RMW < r \leq 4 \times RMW \tag{2}$$

$$V_w = V_{NCEP}, r > 4 \times RMW \tag{3}$$

where r is the radial distance from the typhoon center, V_{NCEP} is the background wind speed and *ntimes* is a parameter to be modified. When *ntimes* equals 1, the formulas give the original NCEP wind. We calculate the maximum wind radial distance using the NCEP wind data with the center location provided by the Typhoon Online of China (http://www.typhoon.gov.cn/). Then, the maximum wind radial distance was treated as the *RMW* to construct the horizontal wind fields, neglecting asymmetry. We modify the wind forcing using Equations (1) to (3) for the period from 9 October to 11 October, by choosing the *ntimes* = 1.1, 1.2, 1.3, 1.4 and 1.5, respectively.

2.5. Calibration of the Stom Surge Model against Altimetry Data

De-tided model sea surface heights forced by the NCEP and modified winds are interpolated on to the satellite ground track at the time (05:46 UTC on 10 October 1994) of the satellite passing, one cycle before and one cycle after. To eliminate the impacts of the mean sea surface height difference between the altimetric and model results on the storm surge comparison, we first calculate an average from Cycle 75 (07:48 UTC, 30 September 1994) and 77 (03:44 UTC, 20 October 1994) and then subtract the average from sea surface height of Cycle 76. This procedure is applied to the model and altimetric results, respectively. We calculate the root-mean–square (RMS) difference between the altimetric and model results for each *ntimes*. The run with the smallest RMS difference is chosen as the baseline case.

3. Results

3.1. Simulated Tides

The simulated co-tidal chart for the dominant constituent M2 constituent (Figure 3) in the study region agrees generally with the observation-based co-tidal chart in Fang et al. (2004). As can be seen, the M2 tide enhances significantly in Taiwan Strait, with an amplitude greater than 2 m. At the Xiamen (XM) tide-gauge station, the simulated major semi-diurnal and diurnal tidal constituents and shallow-water constituents agree well with the observations (Table 1). The good agreement of the model tides with observations (especially for the shallow-water constituents) suggests that the bottom friction formulation used in the present model is reasonable.

Table 1. Comparison of the amplitude (m) and phase (°) between that simulated and observed at XM.

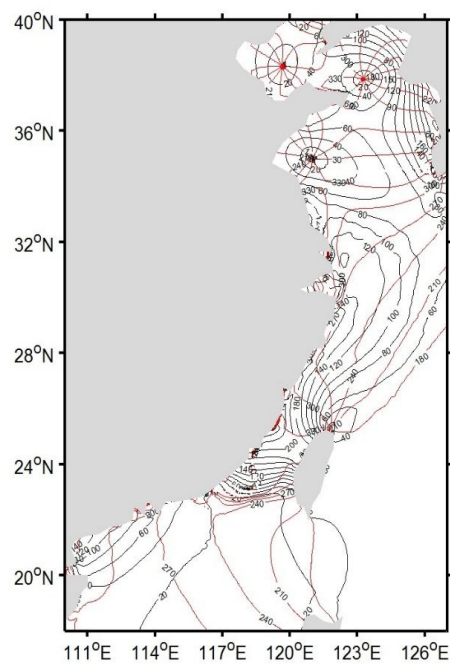| Tide	Simulated Amplitude	Observed Amplitude	Simulated Phase	Observed Phase
Q1	0.06	0.05	120	125
O1	0.30	0.28	128	140
P1	0.11	0.11	162	172
K1	0.35	0.34	163	175
N2	0.30	0.37	112	129
M2	1.67	1.85	132	148
S2	0.52	0.54	169	194
K2	0.14	0.15	156	192
MN4	0.03	0.03	266	289
M4	0.09	0.08	282	309
MS4	0.06	0.05	319	353

Figure 3. M2 co-tidal and co-phase charts from FVCOM. The red and black lines show the phase lag (in degrees relative to Beijing local time (UT + 8 h)) and amplitude (in centimeters), respectively.

3.2. Comparison of Model Storm Surge under NCEP Winds with Tide-Gauge Data

The de-tided model sea surface heights are interpolated to the Xiamen tide-gauge station. Forced by the NCEP wind only, the model significantly underestimates the peak storm surge (Figure 4). The peak storm surge is 1.01 m from the tide-gauge data, but 0.71 m only from the model result, an underestimate of 0.3 m (30%). On the other hand, the model captures the timing of the peak storm surge well, suggesting that both the timing of the NECP wind evolution and the model storm surge propagation speed are realistic. Note that the pole tide is not removed from the tide-gauge storm surge. However, the pole tide is small in magnitude (<1 cm) at the time, and its impact is negligible in the present study.
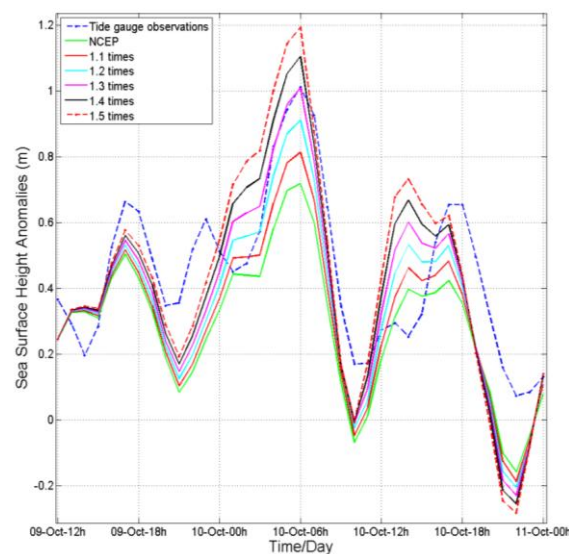

Figure 4. Sea level anomalies comparison between observations and simulations at Xiamen.

3.3. Storm Surge from T/P Observations

The altimetric sea surface height anomalies during Typhoon Seth (Cycle 76, 10 October 1994) increase rapidly from the shelf break (at 22.3°N where the 200-m isobath is located) toward the coast of Fujian (Figure 5). Quality altimetric data are unavailable within about 50 km from the coast. The altimetric sea surface height anomalies reach 0.7 m at the location closest to the coast. In contrast, the altimetric sea surface height anomalies have much smaller cross-shelf variations before (Cycle 75) and after (Cycle 77) Typhoon Seth.
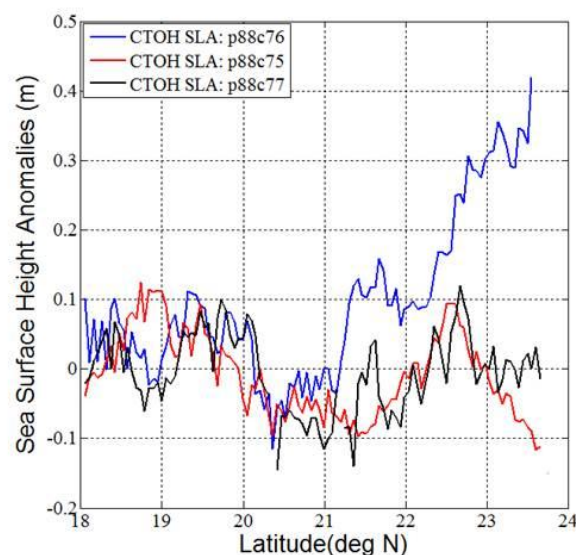

Figure 5. Altimetric sea surface height anomalies along Track 88 observed by T/P. Blue: Cycle 76 during Typhoon Seth. Red: Cycle 75. Black: Cycle 77. CTOH, Centre for Topographic studies of the Ocean and Hydrosphere. SLA, Sea Level Anomalies.

3.4. Comparison of Model Storm Surge under NCEP Winds with T/P Observations

We can see a significant difference between the altimetric and model results, with the model underestimation (Figure 6). Over the continental shelf inshore of 22.3°N, the difference represents the model underestimation of storm surge. The root-mean-square (RMS) difference is 0.15 m (Table 2). In the deep waters offshore of 22.3°N, the difference may in part be attributed to missing baroclinic ocean processes in the present barotropic model, which are present in the altimeter observations. The deep-water region is dynamically complex, with seasonally-varying slope currents, mesoscale eddies and Kuroshio intrusion currents [28]. There may be trapped waves propagating along the shelf break.

Table 2. RMS difference of non-tidal sea level anomalies between the model and T/P observations.

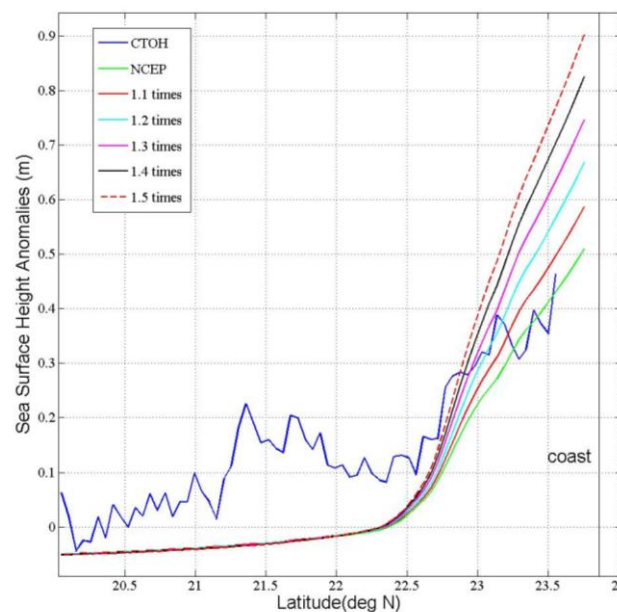|	RMS (22.3 to 23.55°N)
NCEP	0.15 m
modified by 1.1	0.13 m
modified by 1.2	0.11 m
modified by 1.3	0.10 m
modified by 1.4	0.11 m
modified by 1.5	0.12 m

Figure 6. De-tided altimetric and model surface height anomalies for Cycle 76 during Hurricane Seth, relative to those averaged for Cycle 75 and 77.

3.5. Calibration against Altimetric Observations

Because the model forced by the NCEP wind and tide is able to well reproduce major tidal constituents and the shallow-water tidal constituents (see Section 3.1), we can conclude that the model underestimation of the coastal storm surge magnitude is not caused by the bottom friction parameterization. Also because the model captures the timing of the peak storm surge well, we can consider both the timing of the NECP wind evolution and the model storm surge propagation speed realistic. On the other hand, upon examining the NCEP wind speed, we find that the maximum NCEP wind is much lower than the maximum sustained wind of the best-track data. For example, at 6:00 10 October 1994, the maximum NCEP wind is 30.33 m/s. Therefore, we modify the wind forcing using Equations (1)–(3) for the period from 9 October to 11 October, by choosing the *ntimes* = 1.1, 1.2, 1.3, 1.4 and 1.5, respectively. Table 3 shows the differences in the maximum wind speed between the modified results and best-track data. The RMS difference of the maximum wind speed between the modified wind fields and best-track data is smallest at *ntimes* = 1.3 (about 2 m/s), while it is about 10 m/s between the NCEP and observed wind fields (Table 4). Figure 7 shows the wind patterns before and after the modification at 6:00 10 October 10 1994. A further evaluation of the NCEP and modified wind fields against independent weather station data was made at Dachen (Table 5). The results show the smallest mean and RMS differences at *ntimes* = 1.3 − 1.4.

Table 3. Comparison of the maximum wind speed (m/s) between the NCEP, modified and best-track wind fields.

	9 October, T12	9 October, T18	10 October, T00	10 October, T06	10 October, T12	10 October, T18	11 October, T00
NCEP	33	31	29	30	27	22	22
Modified by 1.1	36	34	32	33	30	24	25
Modified by 1.2	40	38	34	36	32	27	27
Modified by 1.3	43	41	37	39	35	29	29
Modified by 1.4	46	44	40	42	38	31	31
Modified by 1.5	49	47	43	45	40	33	33
best-track	45	40	40	40	35	30	30

Table 4. RMS difference in maximum wind speed (m/s) between best-track and modified winds from 12:00 9 October to 00:00 11 October. For NCEP winds, *ntimes* = 1.0.

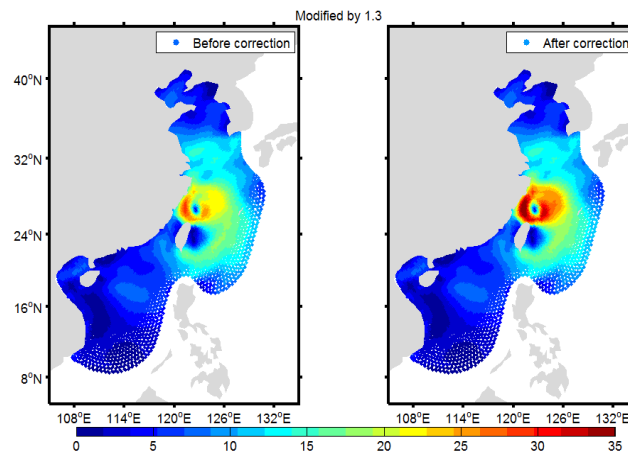| *ntimes*	NCEP	1.1	1.2	1.3	1.4	1.5
RMS	9.6	6.7	3.9	1.6	2.1	4.5

Figure 7. Comparison between the modified and NCEP wind field at 06:00, 10 October.

Table 5. NCEP, modified (*ntimes* = 1.1 to 1.5) and observed wind speed (m/s) at Dachen from 12:00 9 October to 00:00 11 October.

ntimes	9 October, T12	9 October, T18	10 October, T00	10 October, T06	10 October, T12	10 October, T18	11 October, T00	Mean
NCEP	8.9	13.1	15.0	19.1	13.6	14.9	11.9	13.8
1.1	8.9	13.3	15.9	20.5	14.8	16.3	12.8	14.6
1.2	8.9	13.3	16.7	21.9	15.9	17.7	13.7	15.4
1.3	8.9	13.5	17.5	23.4	17.1	19.1	14.6	16.3
1.4	8.9	13.7	18.3	24.9	18.2	20.6	15.5	17.2
1.5	8.9	13.8	19.1	26.3	19.4	21.9	16.4	18.0
Dachen	9.3	12.0	14.0	22	25.0	22	12	16.6

The model results with the modified wind forcing show improved agreement of the model storm surge over the continental shelf inshore of 22.3°N with altimetric data as the *ntimes* increases from one (Figure 6). The best agreement reaches when *ntimes* is 1.3, with the RMS difference reduced to 0.10 m (Table 2).

Finally, we use tide-gauge data as an independent verification of the calibration. When forced by the modified wind (1.3-times the NCEP wind fields) that produces the nearly best agreement with the T/P observations, the model storm surge achieves the best agreement with tide-gauge data at Xiamen (Table 6, Figure 4), in terms of the RMS difference and the peak surge magnitude. Therefore, we choose the model run forced by both the tide and the 1.3-times the NCEP wind fields as the baseline run for further discussion in the next section.

Table 6. RMS difference of non-tidal sea level anomalies between the model and tide-gauge observations at Xiamen.

	RMS
NCEP	0.21 m
modified by 1.1	0.19 m
modified by 1.2	0.18 m
modified by 1.3	0.18 m
modified by 1.4	0.19 m
modified by 1.5	0.21 m

4. Discussion

4.1. Effect of Tide-Surge Nonlinear Interactions

Both model results and tide-gauge data show a significant 12-h oscillation in non-tidal sea level anomalies at the Xiamen tide-gauge station. To understand this oscillation, we have run a model simulation without tides. The model run without tides does not show the 12-h oscillation at all (Figure 8). Therefore, the 12-h oscillation is associated with the nonlinear interactions between the wind-driven storm surge and the tides. The tide-surge interactions in Taiwan Strait were discussed by Zhang et al. (2010) [17], attributable mainly to the bottom friction and advection. In addition, the highest surge of 0.70 m in the simulation without tides occurs about 1 h earlier. At the time of the peak storm surge, the non-linear interactions contribute by 0.34 m (Figure 8) and the pure wind effects by 0.67 m.
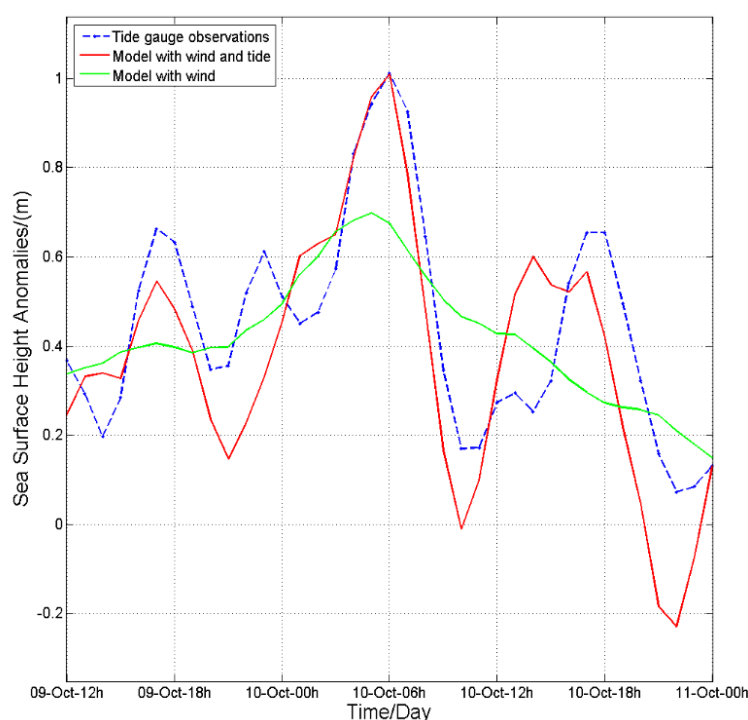

Figure 8. Non-tidal sea surface height anomalies at Xiamen from tide-gauge observations, from the model run forced by the National Center for Atmospheric (NCAR) wind modified by 1.3-times and from the model run forced by both the tide and the NACR wind modified by 1.3-times.

The sea level anomalies due to the nonlinear interactions are negatively correlated with the tide height, that is high tides tend to reduce storm surge and vice versa (Figure 9). The peak positive and negative nonlinear effects are behind the low and high tides, respectively, suggesting that the nonlinear interactions are mainly associated with the bottom friction. The correlation coefficients from 06:00 8 October to 06:00 12 October are -0.46 ($p < 0.001$) at both XM and Pingtan (PT). A numerical study by Rego and Li. [2010] showed a similar relationship between surge and tides in the Gulf of Mexico [29].
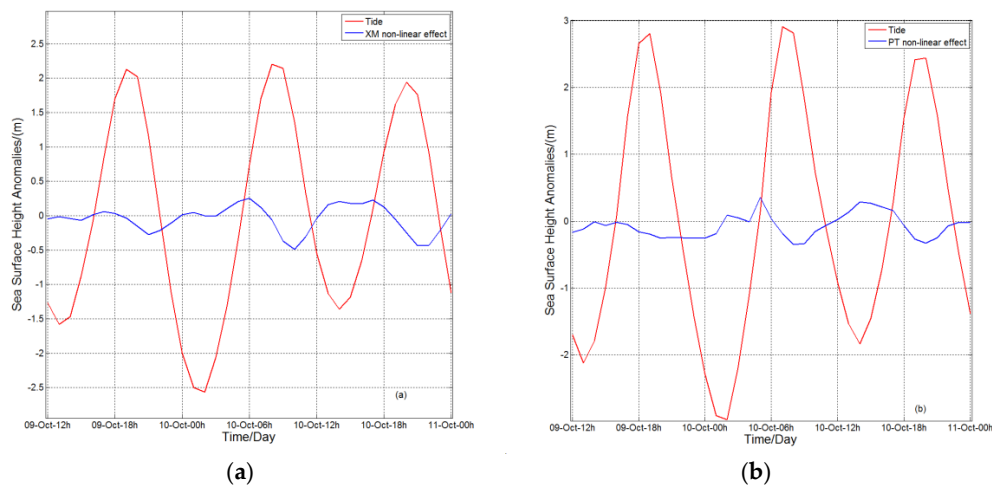
Figure 9. Sea surface height anomalies due to the tide-surge nonlinear interactions and tidal height at (**a**) XM and (**b**) PT. The model is forced by both the tide and the NCEP wind modified by 1.3-times.

4.2. Storm Surge as a Coastally-Trapped Kelvin Wave

The de-tided model sea level anomalies from 03:00 to 08:00 on 10 October 1994 (Figure 10) indicate a storm surge generated along the coast of Fujian, when the typhoon was located northeast of Taiwan. They also showed a southwestward propagation of storm surge. The sea level anomalies were relatively high near the Pingtan tide-gauge station at 03:00 on 10 October (Figure 10a). The high sea level anomalies propagated southwestward, arriving at the Xiamen tide-gauge station at 06:00 (Figure 10d) and at the Dongshan tide-gauge station 2 h later.
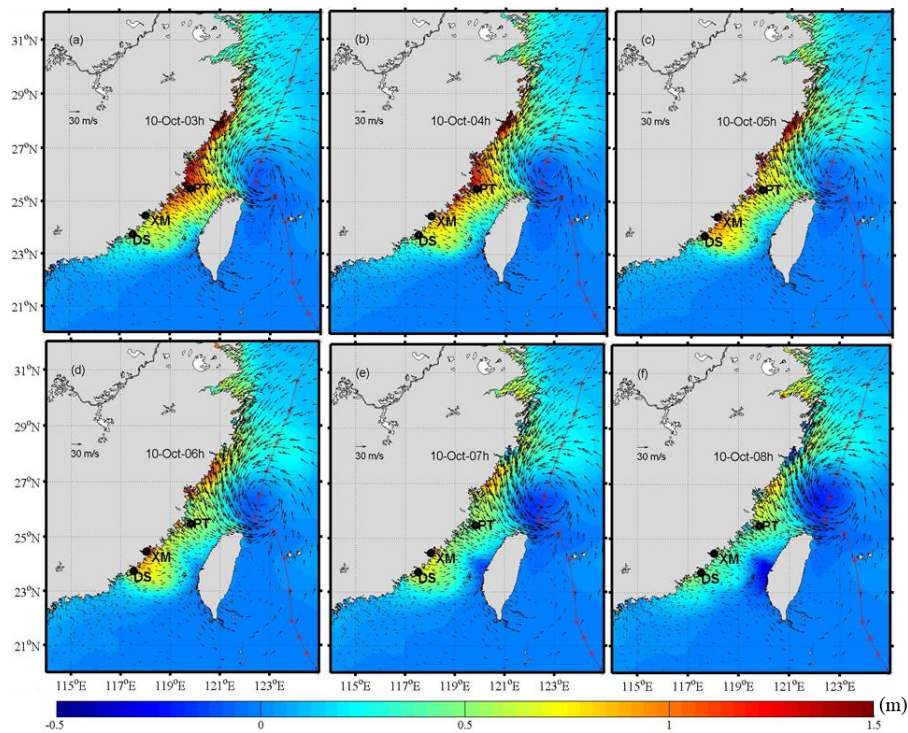

Figure 10. (**a–f**) show temporal change of the model non-tidal sea surface height anomalies and the forcing wind fields at 03:00, 04:00, 05:00, 06:00, 07:00 and 08:00 on 10 October. The model run is forced by both the tide and the NCEP wind modified by 1.3-times.

The coastally-trapped waves are often generated by a passing storm, which propagate along the coast with the coastline on its right in the Northern Hemisphere. We analyze the correlation of the simulated sea level anomalies at Pingtan, Xiamen and Dongshan. Xiamen is used as the reference. The lagged correlation coefficients are calculated and shown in Figure 11. The correlation results indicate that it takes 3 h for the storm surge wave to travel from Pingtan to Xiamen and 2 h from Xiamen to Dongshan (Figure 11). The distance between Pingtan and Xiamen is 217 km and between Xiamen and Dongshan is 145 km. Therefore, the propagation speed of the coastally-trapped wave is ~20 m/s, which is consistent with the propagation speed (23 m/s) of the Kelvin wave based on an averaged depth of Taiwan Strait.
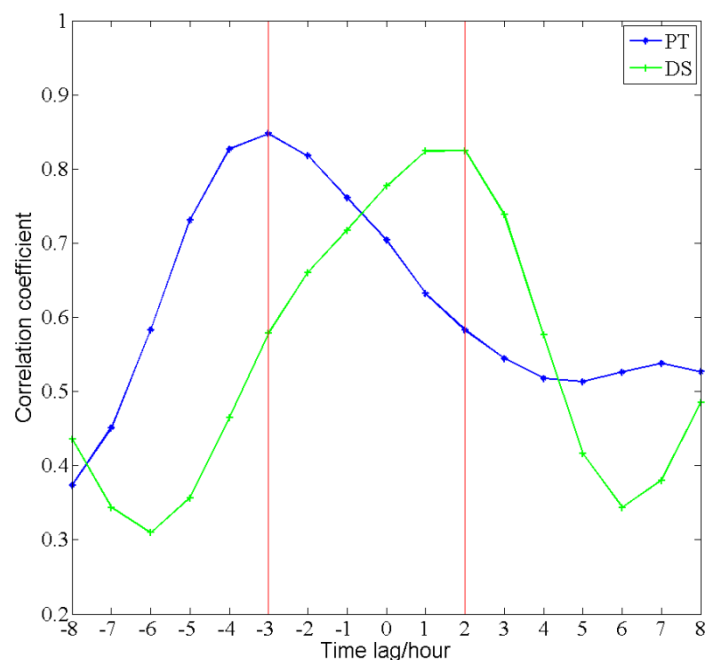

Figure 11. The lagged correlation coefficients of the model non-tidal sea surface height anomalies between PT and XM (blue) and between DS and XM (green). Negative values in the time lag mean the former station leading the latter for each pair. The model run is forced by both the tide and the NCEP wind modified by 1.3-times.

Several previous studies [4,6,10,30,31] have shown that storm surges propagate as first-mode barotropic continental shelf waves. In our case, we calculate the dispersion relationship for a continental shelf wave across a section aligned with the T/P track (Figure 1), based on the barotropic continental shelf wave theory [32]. A continental shelf wave must have a period longer than the local inertial period, which is 29 h at 24.37°N. The dispersion relationship shows that the phase speed of the first-mode continental shelf wave for this area must be less than 8 m/s (Figure 12). The storm surge signal during Seth has a dominant period of 12 h (shorter than the shortest possible period of 29 h for a continental shelf wave) and a propagating phase speed of ~20 m/s (greater than the greatest possible phase speed of 8 m/s for a continental shelf wave); therefore, it is impossible for it to be a continental shelf wave.
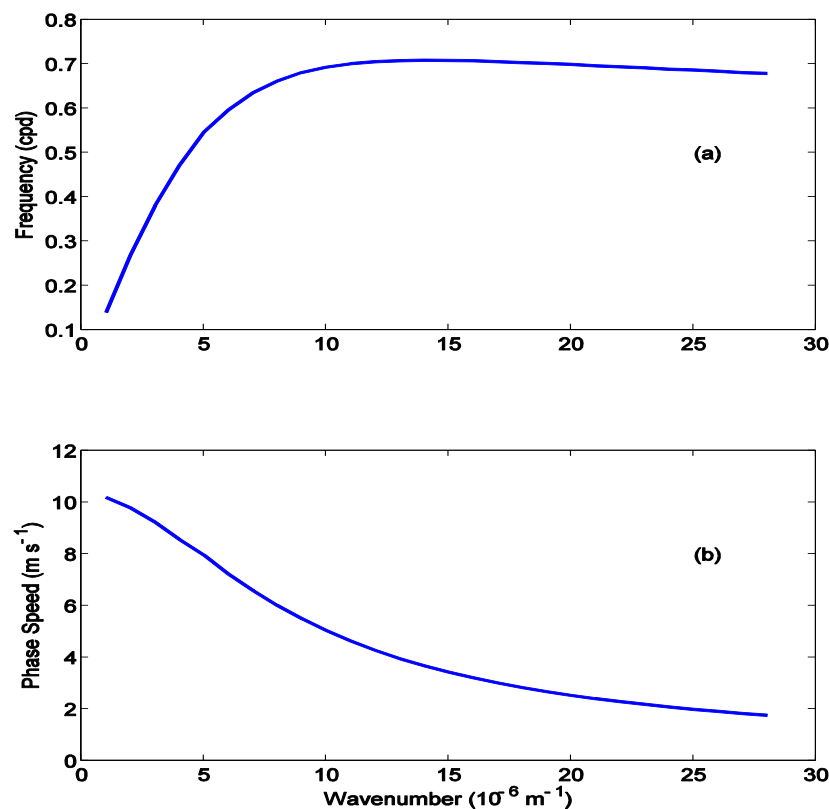
Figure 12. (**a**) The dispersion relationship estimated for the first-mode continental shelf wave in the coastal area nearby the T/P ground track; (**b**) the corresponding wave speed curve.

4.3. Strength and Limitation

In the present study, the calibrated model produced the storm surge in good agreement with the tide-gauge observations. The study points to the usefulness of altimetric data in improving storm surge modelling, with its cross-shore information making up for the limitation of a one-time single profile. Such an altimetric profile would be particularly useful for regions lacking tide-gauge observations. The model results are used to explain the impacts of tide-surge interactions and the alongshore propagation of storm surge. However, the altimeter data are used to adjust the wind forcing in an ad hoc way, instead of being dynamically assimilated into the storm surge model. Though the underestimation of typhoon winds in the reanalysis product is a general issue, the degree of underestimation varies storm by storm and is difficult to generalize. We also recognize that the present study provides one single case only. More cases are needed to demonstrate the improvements from a statistical perspective in the future.

The present study adjusts the wind forcing field in reference to the typhoon best-track data to minimize model-altimetry mismatch. This approach is simple and is proven to work well with the pre-determination that the underestimation of Typhoon Seth wind speed by the NCEP product is the main cause of the model deficiency. Some recent studies [11–13] have used another approach that uses altimetry to improve initial conditions and scatterometry to correct wind fields. Their approach corrects the bias of the global model wind field in reference to scatterometer winds and dynamically assimilates altimetric sea level data to provide a realistic initial state to begin the model simulation. Therefore, the latter approach, though methodologically complex and computationally more expensive, is of more general use and thus is to be pursued in the future.

5. Conclusions

A 3D, barotropic, finite-volume coastal ocean model was developed to simulate and study the storm surge along the southeastern China during Typhoon Seth in October 1994. A novel aspect is that the model storm surge was calibrated against a TOPEX/Poseidon observed cross-shelf storm surge profile, by adjusting the model wind forcing fields in reference to the typhoon best-track data. Through the calibration process, we determined the baseline wind forcing fields, i.e., 1.3-times the NCEP wind fields, which agree approximately with the best-track data for the maximum sustained speed while have a spatial structure similar to the NCEP wind fields.

The model results from the baseline wind fields reduce the along-track RMS difference between the model and altimetric data from 0.16 m to 0.09 m. It reduces the RMS temporal difference from 0.21 m to 0.18 m between model and tide-gauge data at Xiamen. In particular, the baseline model produces a peak storm surge of 1.01 m at 6:00 10 October 1994 at Xiamen, agreeing with tide-gauge data. The model results also show that the nonlinear interactions between the storm surge and astronomical tides contribute to the peak storm surge by 34% and that the storm surge propagates southwestward as a coastally-trapped Kelvin wave.

Author Contributions: G.H., J.Y., and D.C. conceived the idea and designed the approach. X.L. implemented and ran the model, as well as analyzed the data, under the close guidance of G.H. and J.Y. G.Z. and N.C. contributed to the data analysis. X.L. and G.H. wrote the paper. J.Y. and D.C. contributed to the paper writing.

Conflicts of Interest: The authors declare no conflict of interest.

References

1. Brown, J.D.; Spencer, T.; Moeller, I. Modeling storm surge flooding of an urban area with particular reference to modeling uncertainties: A case study of Canvey Island, United Kingdom. *Water Resour. Res.* **2007**, *43*, W6402. [CrossRef]

2. Price, J.F. Upper Ocean Response to a Hurricane. *J. Phys. Oceanogr.* **1981**, *2*, 153–175. [CrossRef]

3. Sanford, T.B.; Black, P.G.; Haustein, J.R.; Feeney, J.W.; Forristall, G.Z. Ocean Response to a Hurricane. Part I: Observations. *J. Phys. Oceanogr.* **1987**, *11*, 2065–2083. [CrossRef]

4. Han, G.; Ma, Z.; Chen, D.; Deyoung, B.; Chen, N. Observing storm surges from space: Hurricane Igor off Newfoundland. *Sci. Rep.* **2012**, *2*, 1010. [CrossRef] [PubMed]

5. Shutler, J.D.; Quartly, G.D.; Donlon, C.J.; Sathyendranath, S.; Platt, T.; Chapron, B.; Johannessen, J.A.; Girard-Ardhuin, F.; Nightingale, P.D.; Woolf, D.K.; et al. Progress in satellite remote sensing for studying physical processes at the ocean surface and its borders with the atmosphere and sea ice. *Prog. Phys. Geogr.* **2016**, *40*, 215–246. [CrossRef]

6. Chen, N.; Han, G.; Yang, J.; Chen, D. Hurricane Sandy storm surges observed by HY-2A satellite altimetry and tide-gauges. *J. Geophys. Res. Oceans* **2014**, *119*, 4542–4548. [CrossRef]

7. Scharroo, R.; Smith, W.; Lillibridge, J.L. Satellite altimetry and the intensification of Hurricane Katrina. *Eos Trans. Am. Geophys. Union* **2005**, *40*, 366. [CrossRef]

8. Lillibridge, J.; Lin, M.; Shum, C.K. Hurricane Sandy Storm Surge Measured by Satellite Altimetry. *Oceanography* **2013**, *2*, 8–9. [CrossRef]

9. Fenoglio-Marc, L.; Scharroo, R.; Annunziato, A.; Mendoza, L.; Becker, M. Cyclone Xaver seen by geodetic observations. *Geophys. Res. Lett.* **2015**, *22*, 9925–9932. [CrossRef]

10. Han, G.; Ma, Z.; Chen, N.; Chen, N.; Yang, J. Hurricane Isaac storm surges off Florida observed by Jason-1 and Jason-2 satellite altimeters. *Remote Sens. Environ.* **2017**, *198*, 244–253. [CrossRef]

11. De Biasio, F.; Bajo, M.; Vignudelli, S.; Umgiesser, G.; Zecchetto, S. Improvements of storm surge forecasting in the Gulf of Venice exploiting the potential of satellite data: The ESA DUE eSurge-Venice project. *Eur. J. Remote Sens.* **2017**, *50*, 428–441. [CrossRef]

12. Bajo, M.; De Biasio, F.; Umgiesser, G.; Vignudelli, S.; Zecchetto, S. Impact of using scatterometer and altimeter data on storm surge forecasting. *Ocean Model.* **2017**, *113*, 85–94. [CrossRef]

13. De Biasio, F.; Vignudelli, S.; Della Valle, A.; Umgiesser, G.; Bajo, M.; Zecchetto, S. Exploiting the Potential of Satellite Microwave Remote Sensing to Hindcast the Storm Surge in the Gulf of Venice. *IEEE J. Sel. Top. Appl. Earth Obs. Remote Sens.* **2016**, *9*, 5089–5105. [CrossRef]

14. Ye, A.; Chen, Z.; Yu, Y. Numerical inverstigation of three-dimensional semidiurnal tidal waves in Taiwan Strait and its adjacent areas. *Oceanol. Limnol. Sin.* **1985**, *6*, 439–450.

15. Li, Y.; Cai, W.; Li, L.; Lin, M. The tide characteristics of the seas adjacent to Fujian and Taiwan derived from TOPEX/POSEIDON altimeter data. *Acta Oceanol. Sin.* **2002**, *24*, 154–162.

16. Zhang, W.Z.; Hong, H.S.; Shang, S.P.; Chen, D.W.; Chai, F. A two-way nested coupled tide-surge model for the Taiwan Strait. *Cont. Shelf Res.* **2007**, *27*, 1548–1567. [CrossRef]

17. Zhang, W.Z.; Shi, F.; Hong, H.S.; Shang, S.P.; Kirby, J.T. Tide-surge Interaction Intensified by the Taiwan Strait. *J. Geophys. Res.* **2010**. [CrossRef]

18. Prandle, D.; Wolf, J. Surge-Tide Interaction in the Southern North Sea. In *Elsevier Oceanography Series*; Elsevier: New York, NY, USA, 1978; pp. 161–185.

19. Zhen, W.; Chen, F.; Chen, X. Tides and tidal currents in the Taiwan Strait. *J. Oceanogr. Taiwan Strait* **1982**, *2*, 1–4.

20. Pan, H.; Liu, F. A numerical study of the tide-surge interaction in the East China Sea and the South China Sea. *Chin. J. Oceanol. Limnol.* **1994**, *1*, 13–21.

21. Chen, C.; Liu, H.; Beardsley, R.C. An Unstructured Grid, Finite-Volume, Three-Dimensional, Primitive Equations Ocean Model: Application to Coastal Ocean and Estuaries. *J. Atmos. Ocean. Technol.* **2003**, *20*, 159–186. [CrossRef]

22. Birol, F.; Fuller, N.; Lyard, F.; Cancet, M.; Nino, F.; Delebecque, C.; Fleury, S.; Toublanc, F.; Melet, A.; Saraceno, M.; et al. Coastal Applications from Nadir Altimetry: Example of the X-TRACK Regional Products. *Adv. Space Res.* **2016**. [CrossRef]

23. Pawlowicz, R.; Beardsley, B.; Lentz, S. Classical tidal harmonic analysis including error estimates in MATLAB using T_TIDE. *Comput. Geosci.* **2002**, *28*, 929–937. [CrossRef]

24. Amante, C.; Eakins, B.W. ETOPO1 1 Arc-Minute Global Relief Model_Procedures, Data Sources and Analysis. *NOAA Tech. Memo. NESDIS NGDC-24* **2008**. [CrossRef]

25. Egbert, G.D.; Erofeeva, S.Y. Efficient Inverse Modeling of Barotropic Ocean Tides. *J. Atmos. Ocean. Technol.* **2002**, *19*, 183–204. [CrossRef]

26. Weisberg, R.H.; Zheng, L. Circulation of Tampa Bay driven by buoyancy, tides and winds, as simulated using a Finite Volume Coastal Ocean Model. *J. Geophys. Res.* **2008**, *111*, C1005. [CrossRef]

27. Ma, Z.; Han, G.; de Young, B. Oceanic responses to hurricane Igor over the Grand Banks: A modelling study. *J. Geophys. Res. Oceans* **2015**, *120*. [CrossRef]

28. Su, J.; Yuan, Y. (Eds.) *Hydrography in the Chinese Seas*; Ocean Press: Beijing, China, 2005; p. 367. (In Chinese)

29. Rego, J.O.L.; Li, C. Nonlinear terms in storm surge predictions: Effect of tide and shelf geometry with case study from Hurricane Rita. *J. Geophys. Res.* **2010**, *115*. [CrossRef]

30. Tang, C.L.; Gui, Q.; De Tracey, B.M. Barotropic response of the Labrador/Newfoundland Shelf to a moving storm. *J. Phys. Oceanogr.* **1998**, *17*, 1152–1172. [CrossRef]

31. Thiebaut, S.; Vennell, R. Observation of a fast continental shelf wave generated by a storm impacting Newfoundland using wavelet and cross-wavelet analyses. *J. Phys. Oceanogr.* **2010**, *40*, 417–428. [CrossRef]

32. Brink, K.H.; Chapman, D.C. *Programs for Computing Properties of Coastal-Trapped Waves and Wind-Driven Motions over the Continental Shelf and Slope*; WHOI Tech. Rep. WHOI-87-24; Woods Hole Oceanographic Institution: Woods Hole, MA, USA, 1987; 119p.